

Chemical Abundances in the Secondary Star in the Black Hole Binary A0620–00

Jonay I. González Hernández, Rafael Rebolo,¹
Garik Israelian, and Jorge Casares

Instituto de Astrofísica de Canarias, E-38205 La Laguna, Tenerife, SPAIN:
jonay@ll.iac.es, rrl@ll.iac.es, gil@ll.iac.es, jcv@ll.iac.es

and

Andre Maeder and Georges Meynet

Geneva Observatory, 1290 Sauverny, SWITZERLAND:
Andre.Maeder@obs.unige.ch, Georges.Meynet@obs.unige.ch

ABSTRACT

Using a high resolution spectrum of the secondary star in the black hole binary A0620–00, we have derived the stellar parameters and veiling caused by the accretion disk in a consistent way. We have used a χ^2 minimization procedure to explore a grid of 800 000 LTE synthetic spectra computed for a plausible range of both stellar and veiling parameters. Adopting the best model parameters found, we have determined atmospheric abundances of Fe, Ca, Ti, Ni and Al. The Fe abundance of the star is $[\text{Fe}/\text{H}] = 0.14 \pm 0.20$. Except for Ca, we found the other elements moderately over-abundant as compared with stars in the solar neighborhood of similar iron content. Taking into account the small orbital separation, the mass transfer rate and the mass of the convection zone of the secondary star, a comparison with element yields in supernova explosion models suggests a possible explosive event with a mass cut comparable to the current mass of the compact object. We have also analyzed the Li abundance, which is unusually high for a star of this spectral type and relatively low mass.

Subject headings: black holes physics—stars:abundances—stars:individual (A0620-00)—stars:X-rays:low-mass—binaries

¹Consejo Superior de Investigaciones Científicas, SPAIN

1. Introduction

The system A0620–00 (V616 Mon) is a low mass X-ray binary (LMXB) discovered as an eruptive X-ray source by *Ariel V* in August 1975 (Elvis et al., 1975). During the outburst, it brightened by 6 magnitudes in the optical and after 15 months it had returned to its quiescent magnitude of $m_V = 18.3$ mag. Spectroscopic observations during quiescence revealed a K5 V–K7 V stellar spectrum plus an emission line component from an accretion disk surrounding the compact object (Oke 1977; Murdin et al., 1980). Further optical photometric and spectroscopic studies established the orbital period at $P = 0.323$ d and a secondary radial velocity semiamplitude of $K_2 = 457$ km s $^{-1}$ (McClintock & Remillard 1986), which implied a mass function of $f(M) = 3.18 \pm 0.16 M_\odot$ and thus firm dynamical evidence for a massive compact object—a black hole—in this system. From measurements of the orbital inclination, the compact object mass was estimated at $\sim 11 M_\odot$ and the companion star mass at $\sim 0.7 M_\odot$ (Shahbaz et al., 1994; Gelino et al., 2001).

Many aspects of the origin and evolution of low mass X-ray binaries (LMXBs) still remain unclear. It is believed that these systems begin as wide binaries with extreme mass ratios and orbital separations of $a \sim 1000 R_\odot$ (Portegies Zwart et al., 1997; Kalogera & Webbink 1998). After filling its Roche lobe, the massive star engulfs its low mass companion and the latter starts to spiraling in to the massive star’s envelope (van den Heuvel & Habets 1984; de Kool et al., 1987). A close binary forms if the spiral-in ceases before the low mass companion coalesces with the compact helium core of the primary. The helium core continues its evolution and after SN explosion may turn into a neutron star or a black hole. The system becomes an X-ray binary once the secondary star fills its Roche lobe and begins to transfer matter to the compact object.

The spiral-in process could give rise to a naked He core, identified with Wolf–Rayet stars that have lost their envelopes (Woosley et al., 1995). The high mass-loss rate (Chiosi & Maeder 1986; Nugis & Lamers 2000) of these stars makes difficult to understand the formation of compact objects as massive as the black hole in A0620–00 (Meynet & Maeder 2003; Woosley et al., 1993). However, if the hydrogen envelope of the massive star is removed at the end of the He core burning phase (the so-called *Case C* mass transfer, Brown et al., 1999), the mass lost by wind in the short-lived ($\sim 10^4$ yr) supergiant stage will not be large.

Convection (Langer 1991) and rotation (Maeder & Meynet 2000; Heger et al., 2000) influence the structure and evolution of massive stars and subsequently the uncertainties in the treatment of these parameters limit our understanding of the evolution of the progenitors of compact objects. In addition, uncertainties in various aspects of the supernova explosion models affect the predictions of the final remnant mass and the chemical composition of any ejecta captured by the companion. Among the least known ingredients of these models, we

may list:

- The *mass cut*, i.e. the mass above which the matter is expelled at the time of the supernova explosion and below which it remains locked into the compact remnant.
- The *amount of fallback* or of the mass which is eventually accreted by the compact core (Woosley & Weaver 1995; MacFadyen et al., 2001).
- Possible *mixing* during the collapse phase (Herant & Woosley 1994; Herant et al., 1994; Kifonidis et al., 2000; Fryer & Warren 2002).
- The energy of the supernova explosion (Nakamura et al., 2001).
- The symmetry of the supernova explosion (MacFadyen & Woosley 1999; Maeda et al., 2002).

With the aim of obtaining information on the link between compact objects and their progenitor stars, Israelian et al. (1999) measured element abundances in the secondary star of the black hole binary Nova Scorpii 1994 (GRO J1655–40) and found several α -elements (O, Mg, Si, S, and Ti) enriched by a factor of 6–10. Since these elements cannot be produced in a low mass secondary star, this was interpreted as evidence of a supernova event that originated the compact object. Taking into account the supernova yields from explosion models of massive stars, the relative abundances of these elements suggested that the supernova progenitor was in the mass range 25–40 M_{\odot} . Afterwards, these over-abundances were compared with a variety of supernova models, including standard as well as hypernova models (for various helium star masses, explosion energies, and explosion geometries) and a simple model of the evolution of the binary and the pollution of the secondary (Brown et al., 2000; Podsiadlowski et al., 2002). Additional independent evidence for the existence of a supernova event in this system has also been found by Mirabel et al. (2002).

In this paper we analyze the chemical abundances of the secondary star in the LMXB A0620–00 with the aim of searching for any evidence of nucleosynthetic products from the progenitor of the compact object.

2. Observations

2.1. Stellar Spectrum

The secondary star was observed with the UV–Visual Echelle Spectrograph (UVES) at the Very Large Telescope (VLT) of the European Southern Observatory (Paranal), using a

configuration that provided a dispersion 0.029 \AA/pixel in the blue arm ($4800\text{--}5800 \text{ \AA}$) and 0.035 \AA/pixel in the red ($5800\text{--}6800 \text{ \AA}$). Short exposures ($480\text{--}540 \text{ s}$) were chosen in order to avoid as far as possible the smearing of spectral lines associated with radial velocity change during its orbital motion. Twenty spectra were obtained during three nights in December 2000 in both the blue and the red spectral regions.

Every spectrum was reduced within the MIDAS UVES environment. First, bias and inter-order backgrounds were subtracted from both the science and flat-field frames. The spectrum of the target was then optimally extracted and divided by the flat-field (extracted with the same weighted profile as the star). The final spectra were wavelength-calibrated, every order was extracted, and all were merged in order to obtain a one dimensional spectrum for each spectrum.

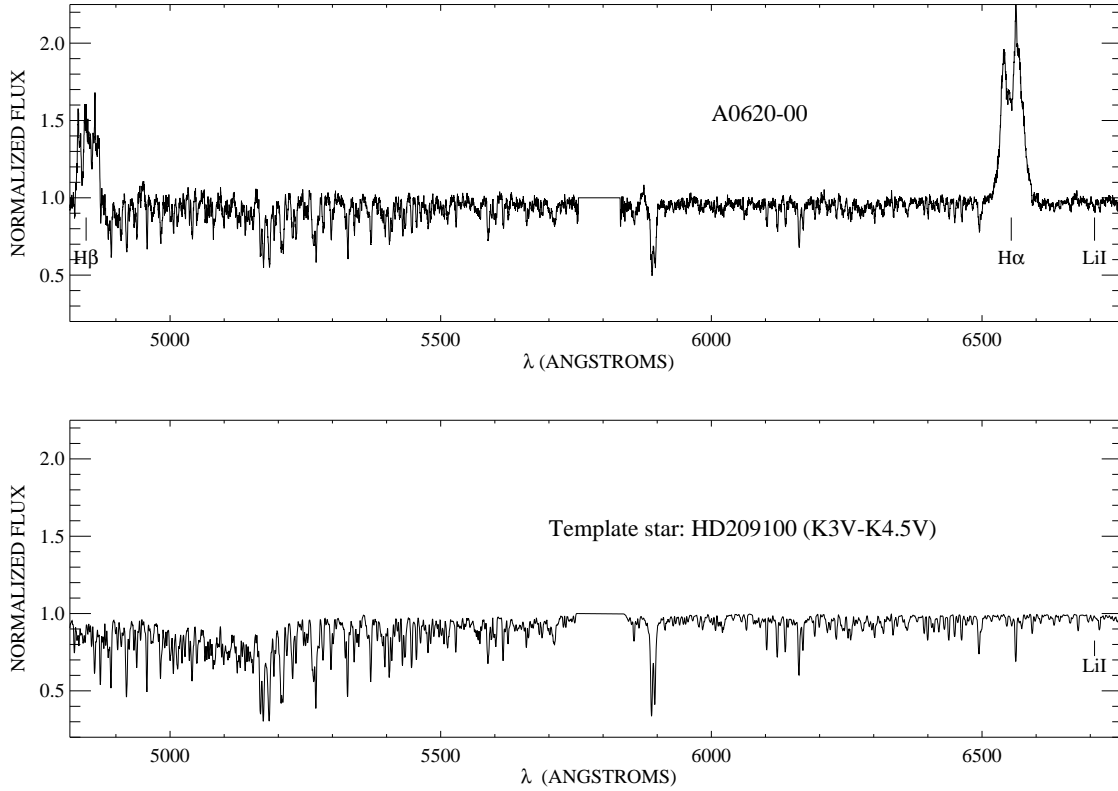


Fig. 1.— Observed spectrum of the secondary star of A0620–00 (top) and of a properly broadened template (HD209100, bottom).

The radial velocity for each spectrum has been obtained from the ephemeris reported in Casares et al. (2004, in preparation). The individual spectra were corrected from radial velocity and combined in order to improve the signal-to-noise ratio. After binning in

wavelength in groups of 10 pixels the final spectrum had a signal-to-noise ratio of 85 in the continuum. This spectrum is shown in Fig. 1.

2.2. Telluric Spectrum

We obtained a telluric spectrum from our own observations and the stellar spectrum was properly corrected for it. The large difference in broadening between the stellar ($\sim 95 \text{ km s}^{-1}$) and telluric lines ($\sim 9 \text{ km s}^{-1}$, the instrumental resolution), allowed us to fit a cubic spline to the stellar features in the binned spectrum of the star, i.e., the final spectrum displayed in Fig. 1. This fit was sampled to the original dispersion provided by the spectrograph and subtracted from each of the 20 individual unbinned spectra taking into account the radial velocity of the star in each case. We used this dispersion to ensure that the telluric lines would not be smoothed. We obtained 20 residual spectra in which we subtracted the stellar features, and which hence contain only telluric and interstellar medium (ISM) features. The combination of these residual spectra gave a noisy telluric spectrum (spectrum 1) which was cross-correlated with another telluric spectrum (spectrum 2) obtained from a fast rotating star. The correlation function of both spectra was centered on zero velocity.

In order to correct our target observations, we used the much higher S/N telluric spectrum 2 scaled down (with the IRAF¹ task TELLURIC) to the strength of the telluric lines in spectrum 1. This scaled telluric spectrum was shifted according to the radial velocity of the target during each exposure. Then we combined all these shifted spectra to generate a final telluric spectrum in the rest frame of the companion star (spectrum 3), which was subtracted from the final spectrum of the target.

¹IRAF is distributed by National Optical Astronomy Observatory, which is operated by the Association of Universities for Research in Astronomy, Inc., under contract with the National Science Foundation.

Table 1. Ranges and steps of model parameters

Parameter	Range	Step
T_{eff}	4000 K \rightarrow 5300 K	100 K
$\log g$	3.5 \rightarrow 5	0.1
[Fe/H]	-0.8 \rightarrow 1	0.05
f_{4500}	0 \rightarrow 0.4	0.05
m_0	0 \rightarrow -0.00016	-1.778E-05

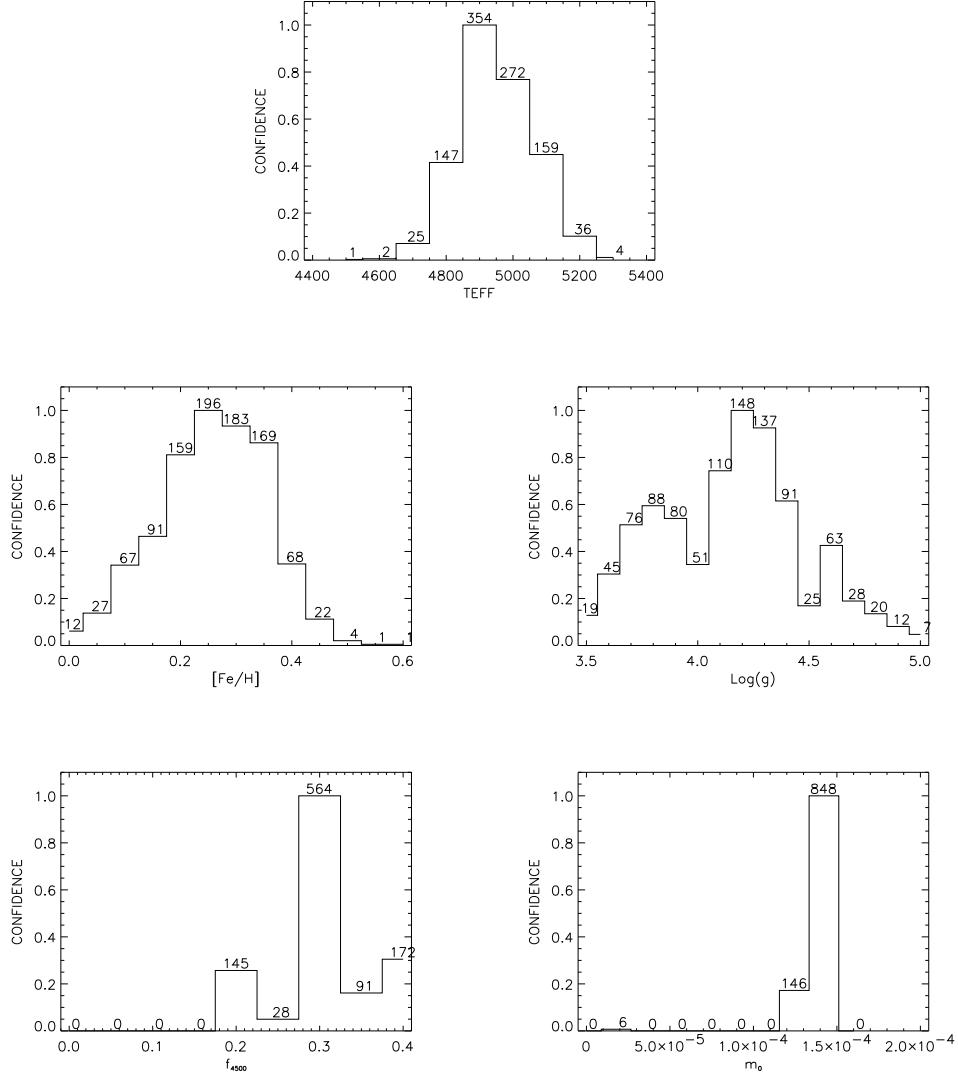


Fig. 2.— Distributions obtained for each parameter using Monte Carlo simulations. The labels at the top of each bin indicate the number of simulations consistent with the bin value. The total number of simulations was 1000.

2.3. Diffuse interstellar bands

In fact, spectrum 1 (see §2.2) does not only consist of telluric lines, it also contains ISM features in the line of sight towards A0620-00. We tentatively identified in this spectrum several of the well known diffuse interstellar bands listed in Herbig (1995). We took care that these bands did not affect the lines selected for the chemical analysis described in the next section.

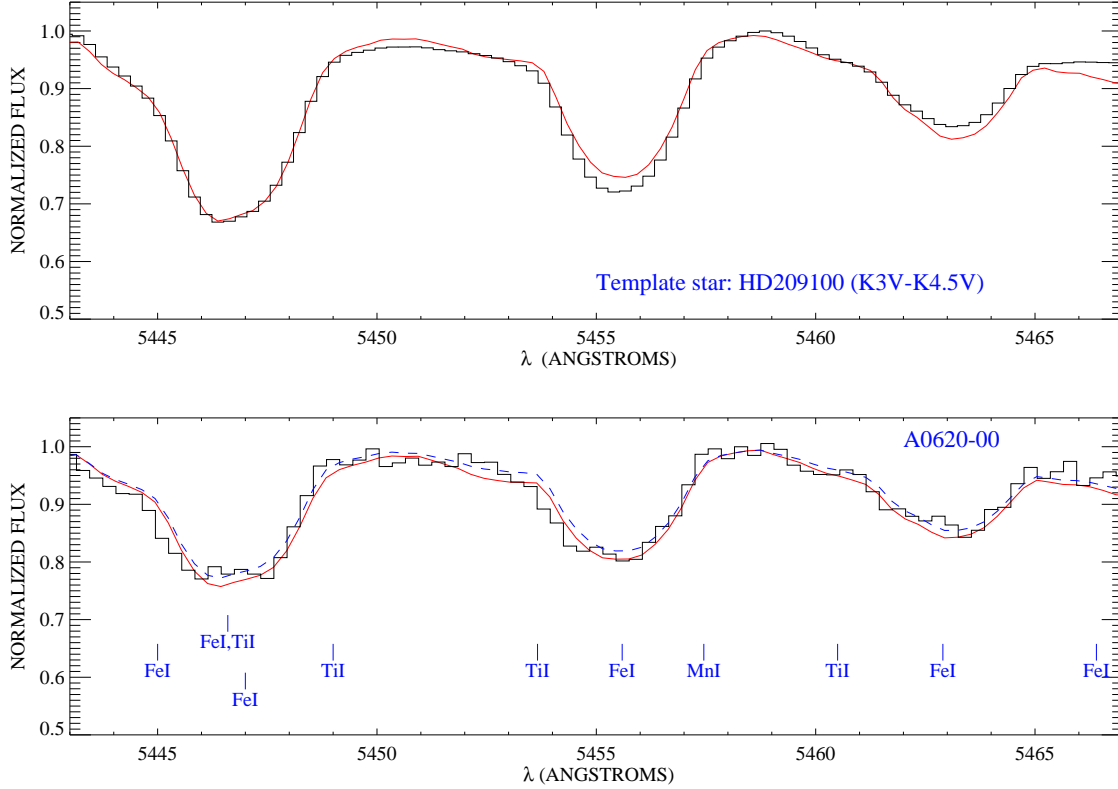


Fig. 3.— Best synthetic spectral fits to the UVES spectrum of the secondary star in the A0620–00 system (bottom panel) and the same for a template star (properly broadened) shown for comparison (top panel). Synthetic spectra are computed for solar abundances (dashed line) and best fit abundance (solid line).

3. Chemical Analysis

3.1. Stellar Parameters

The chemical analysis of secondary stars in LMXB systems is influenced by three important factors: veiling from the accretion disc, rotational broadening, and signal-to-noise ratio. The last two are responsible for the uncertainty in the continuum position and hence affect the normalization procedure. The veiling caused by the accretion disk in A0620–00 appears to drop from the near UV ($\sim 30\%$) to the red ($\sim 6\%$) (Marsh et al., 1994; McClintock & Remillard 2000). However, Shahbaz et al. (1999) have determined that this veiling could be as high as 25% in the IR (K band). All these results depend on the set of templates used, so we decided to attempt an independent determination of the veiling. In our analysis we have

tried to obtain the veiling, together with the stellar atmospheric parameters, using synthetic spectral fits to the high resolution spectrum of the secondary star in A0620–00.

First, moderately strong and relatively unblended lines of several elements of interest were identified in the high resolution solar flux atlas of Kurucz et al. (1984). We selected several spectral features containing in total 24 absorption lines of Fe I with excitation potentials between 0.5 and 4.5 eV. In order to compute synthetic spectra for these features, we adopted the atomic line data from the Vienna Atomic Line Database and used a grid of local thermodynamic equilibrium (LTE) models of atmospheres provided by Kurucz (1992, private communication). These models are interpolated for given values of T_{eff} , $\log g$, and $[\text{Fe}/\text{H}]$. Synthetic spectra were then computed using the LTE code MOOG (Snedden 1973). To minimize the effects associated with the errors in the transition probabilities of atomic lines, we adjusted the oscillator strengths, $\log gf$ values of the selected lines until we succeeded in reproducing the solar atlas of Kurucz et al. (1984) with solar abundances (Anders & Grevesse 1989).

We generated a grid of synthetic spectra for these features in terms of five free parameters three to characterize the star atmospheric model (effective temperature, T_{eff} , surface gravity, $\log g$, and metallicity, $[\text{Fe}/\text{H}]$) and two further parameters to take into account the effect of the accretion disk emission in the stellar spectrum. This veiling was defined as the ratio of the accretion disk flux to the stellar continuum flux, $F_{\text{disc}}/F_{\text{cont,star}}$. It was assumed to be a linear function of wavelength and is thus characterized by two parameters: veiling at 4500 Å, $f_{4500} = F_{\text{disc}}^{4500}/F_{\text{cont,star}}^{4500}$, and the slope, m_0 . These five parameters were changed according to the steps and ranges given in Table 1. Note that the steps for the veiling slope were chosen to cover all possible combinations of veiling at different wavelengths taking into account the step on f_{4500} . A rotational broadening of 95 km s^{-1} and a limb-darkening $\epsilon = 0.65$ were assumed based on Casares et al. (2004, in preparation), and a fixed value for the microturbulence, $\xi = 1 \text{ km s}^{-1}$ was adopted.

The observed spectrum was compared with each of the 800 000 synthetic spectra in the grid via a χ^2 minimization procedure that provided the best model fit. Using a bootstrap Monte-Carlo method we defined the 1σ confidence regions for the five free parameters and established as most likely values: $T_{\text{eff}} = 4900 \pm 100 \text{ K}$, $\log g = 4.2 \pm 0.3$, $[\text{Fe}/\text{H}] = 0.25 \pm 0.1$, $f_{4500} = 0.30 \pm 0.05$, and $m_0 = -0.00014 \pm 0.00002$.

Confidence regions were determined using 1000 realizations. The corresponding histograms are shown in Fig. 2. Our optical veiling determinations are consistent with previous values in the literature for this system (Marsh et al., 1994). These authors found a veiling of 17 ± 3 per cent at $\text{H}\beta$ and $6 \pm 3\%$ at $\text{H}\alpha$, while we have obtained (using their definition for veiling), 20 ± 5 per cent and 0 ± 5 per cent, respectively.

3.2. Stellar Abundances

Using the derived stellar parameters we analyzed several spectral regions where we had identified various lines of Fe, Ca, Al, Ti, Ni, and Li. Although the lines of these elements were usually the main contributor to the features, in some cases, they were blended, mainly with Fe. The inaccuracy in the location of the continuum caused by the blends of many weak rotationally broadened stellar lines was one of the main sources of error in the abundance determinations. Therefore, each of these spectral regions was carefully normalized using a late type star template (HD 209100) for comparison.

We determined the abundances of these elements using spectral synthesis. By comparing the observed spectrum with a grid of synthetic spectra we identified the best fit abundance for each element through a χ^2 minimization procedure. For these spectral syntheses we modified element abundances while stellar parameters and the suitable veiling factor for each spectral region were kept fixed. A preliminary estimate of Fe abundance was obtained in the procedure described above. We then performed a more detailed analysis of the seven Fe dominated spectral features but now taking into account the contribution of much weaker lines to the blends. We obtained an average Fe abundance of $[\text{Fe}/\text{H}] = 0.14 \pm 0.12$, where the error is estimated from the dispersion of the abundances inferred from each feature. A new model with this metallicity was generated in order to perform a detailed spectral synthesis for all the features under consideration.

Abundances for all the elements are listed in Table 2 and referred to the solar values adopted from Anders & Grevesse (1989). We also give errors, estimated from the dispersion of the elemental abundances, Δ_σ , obtained from the best fits to the various features. We have verified that the major source for these errors is the inaccuracy in the location of the continuum caused by the signal-to-noise ratio and the large rotational broadening of the lines. Errors associated with uncertainties in effective temperature, ΔT_{eff} , and gravity, $\Delta \log g$, are also listed in Table 2. The error in the abundance caused by uncertainty in the determination of the veiling is about 0.05 dex for all the elements. We have listed in Table 2 the total error, Δ_{TOTAL} , which takes into account all these sources of uncertainty.

In Fig. 3 we show several Fe spectral features where we can see the best model synthesis in comparison with the synthesis using solar abundances. We also analyzed the spectrum of a template late type star, HD 209100, which was broadened using the rotational profile determined from the spectrum of A0620–00. In the comparison star, the abundances of all the elements studied are close to solar except the Li abundance, which is severely depleted.

Ca and Ni abundances were derived from features where the contribution of these elements was dominant with little blending from other elements, mostly Fe lines. Several Ca

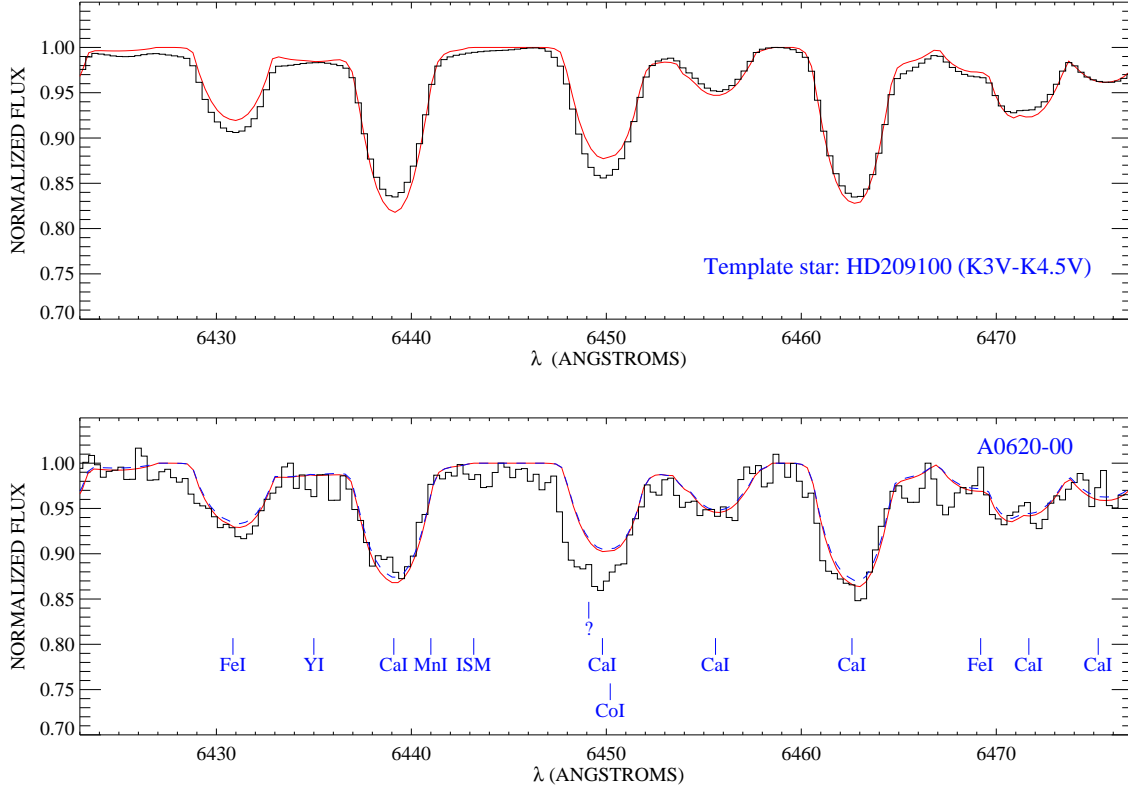


Fig. 4.— The same as in Fig. 3. “?” indicates that there is an unidentified line in the solar spectrum. The label ISM indicates an identified feature produced by the interstellar medium.

spectral features are shown in Fig. 4; in general these features are well reproduced by the synthetic spectra, except for just one, which was blended with an unidentified line in the solar spectrum, and which was not used in the chemical analysis. Ni lines are displayed in Fig. 5. In particular, the unblended moderately strong Ni I line at 6643.6 Å is nicely reproduced by the synthetic spectra.

The selected Ti lines have been corrected for any possible contamination from relatively strong telluric lines ($EW \sim 30$ mÅ compared to the ~ 150 mÅ Ti lines). In Fig. 6, telluric lines are corrected in the spectrum of the secondary star in A0620–00 while in the template these lines (artificially broadened in the convolution) were not subtracted and their presence can be clearly seen.

In Fig. 7 we display the only features of Al and Li investigated, as well as their respective spectral synthesis fits. A comparison is also made with the template star. These are clean

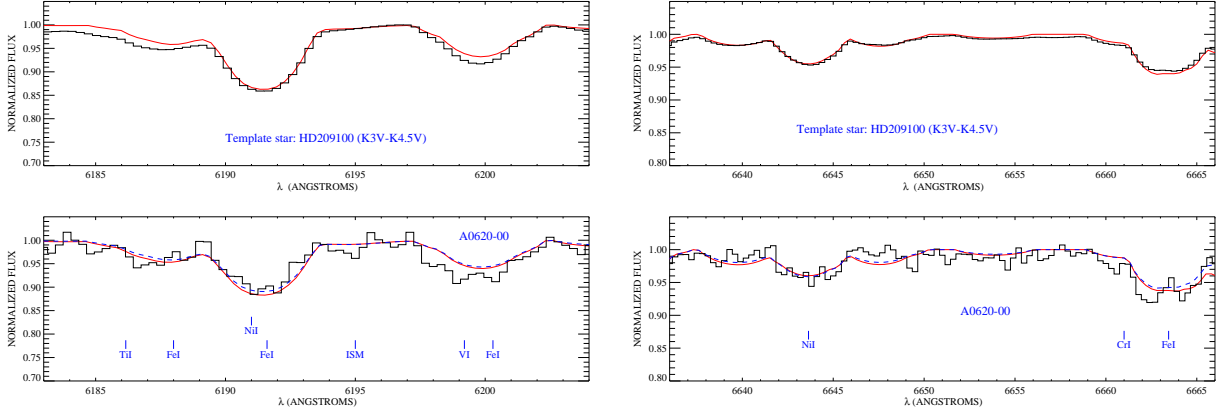


Fig. 5.— The same as in Fig. 3. The Ni line at 6643 Å is one of the very few isolated lines in the spectrum of the secondary star in A0620–00. The label ISM indicates an identified feature produced by the interstellar medium.

weakly blended features where the continuum can be reliably established. The error in the abundances associated with the uncertainty in the continuum location is assumed to be comparable to that of single features in other elements, i.e., 0.1 dex. Li was clearly enhanced with respect the template abundance. The best fit abundance in the template star was $\log \epsilon(\text{Li}) \leq 0.35$ while in the secondary star of A0620–00 it was $\log \epsilon(\text{Li}) = 2.31 \pm 0.21$.

4. Discussion

The abundances of *heavy* elements in the secondary star in A0620–00 are slightly higher than solar. We will examine whether these abundances are anomalous with respect other stars of similar Fe abundance and what abundance ratios would be expected according to a plausible evolutionary scenario for the system.

4.1. Heavy Elements

The Fe abundance of the secondary star is slightly higher than solar but similar to that of many stars in the solar neighborhood. The abundances of other elements listed in Table 2 have to be understood in the context of the chemical evolution of the Galaxy. In Fig. 8 these element abundances relative to iron are shown in comparison with the Galactic abundance trends of these elements in the relevant range of metallicities, taken from Feltzing & Gustafsson (1998) and Bodaghee et al. (2003). The error in the element abundance

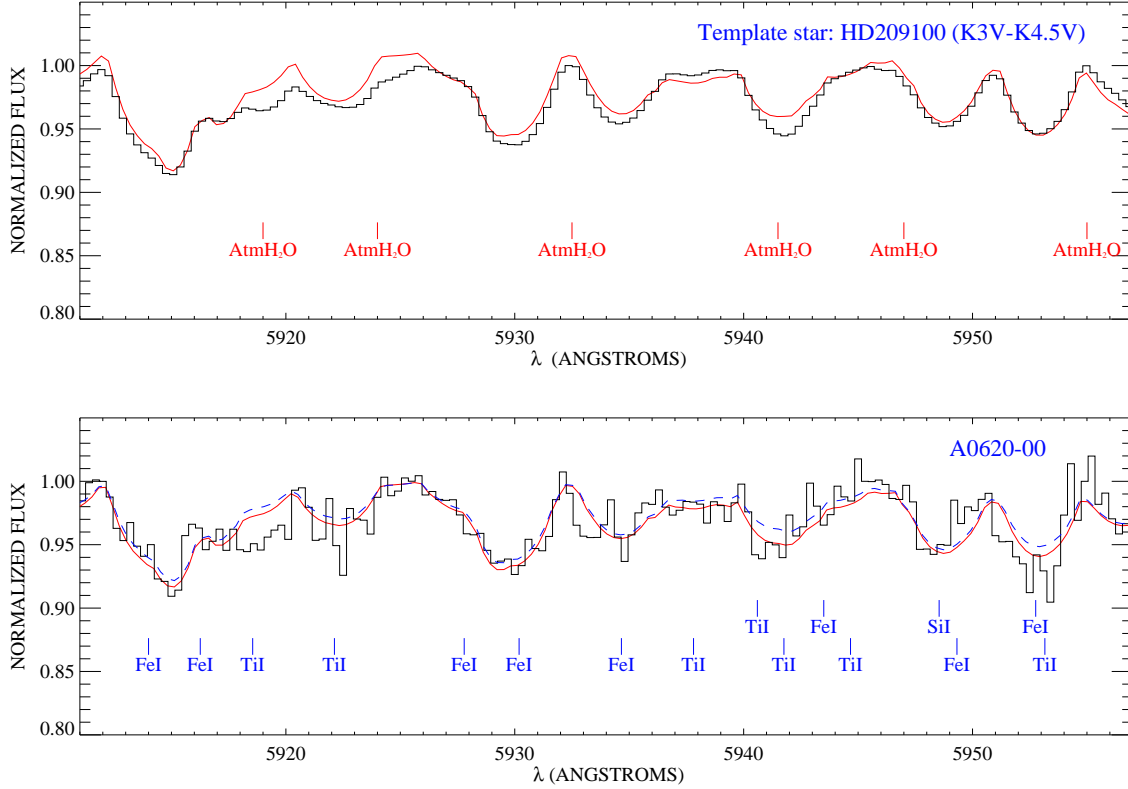


Fig. 6.— The same as in Fig. 3. The spectrum of the template is not corrected for telluric lines (atm. H₂O); therefore, these lines appear broadened in the spectrum (histogram line) and the synthetic spectrum does not fit (solid line).

ratios ($[E/Fe]$) takes into account how individual element abundances depend on the various sources of uncertainty. As can be seen in Table 2, the uncertainties induced by effective temperature and gravity are considerably diminished when dealing with abundance ratios and the major source of error in $[E/Fe]$ is associated with the dispersion, Δ_σ , of abundances obtained from different features of the same element. The $[Ca/Fe]$ ratio of the secondary is consistent with abundances of stars with similar iron content, while Ni and Ti appear to be moderately enhanced. Al is clearly over-abundant if we take into account the low dispersion of Al abundances in these stars. In Table 3 we show the element abundance ratios in the secondary star in A0620–00 and these average values in stars with iron content in the range $-0.06 < [Fe/H] < 0.34$, the comparison sample, corresponding to a 1σ uncertainty in the iron abundance of the companion star. Whereas Ca is consistent with the average values of the comparison sample, Ni, Ti and especially Al are 1σ more over-abundant than the average values of the stars in the comparison sample.

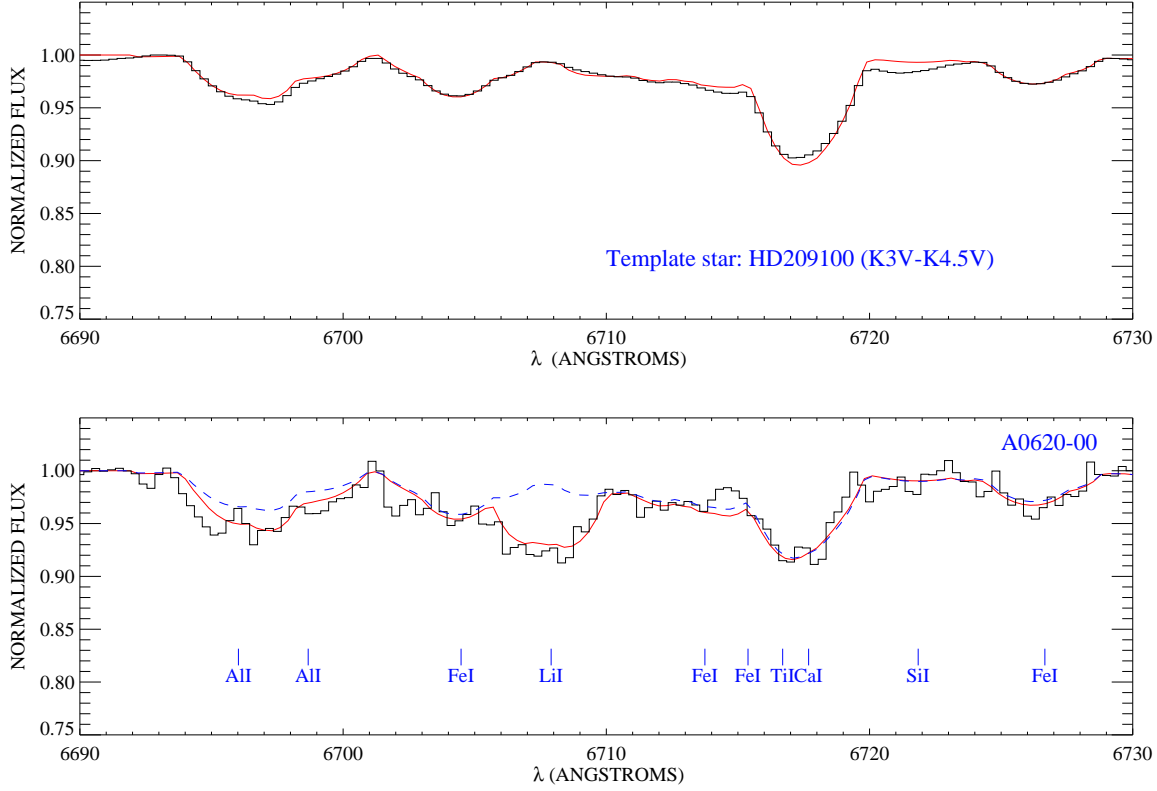


Fig. 7.— The same as in Fig. 3.

We will discuss these results in the framework of possible evolutionary scenarios of the A0620–00 system.

4.1.1. *Evolutionary scenario*

The evolutionary scenario proposed by de Kool et al. (1987) starts with a massive star ($M_1 \sim 40 M_\odot$) and a companion of roughly $M_2 \sim 1 M_\odot$. Spiral-in of the secondary during the red supergiant phase leads to the ejection of the hydrogen-rich envelope and produces a short period helium star binary. In order to be able to reproduce the high mass ($\sim 10 M_\odot$) of the compact object in A0620–00 we should consider the so-called *Case C* for mass transfer in which the massive star does not lose its envelope before finishing its He core burning (Brown et al., 1999). The mass, M_{He} , and radius, R_{He} , of the helium core of the progenitor can be computed using the expressions given by Portegies Zwart et al. (1997,

Table 2. Uncertainties in the abundances of the secondary star in A0620–00

Element	$[E/H]_{\text{LTE}}$	Δ_{σ}	$\Delta_{T_{\text{eff}}}$	$\Delta_{\log g}$	$\Delta_{\text{TOTAL}}^{\dagger}$
Al	0.40	0.10	0.05	-0.05	0.12
Ca	0.10	0.07	0.09	-0.16	0.20
Ti	0.37	0.18	0.10	-0.05	0.23
Fe	0.14	0.12	0.12	-0.08	0.20
Ni	0.27	0.05	0.05	-0.03	0.10
Li*	2.31	0.10	0.15	0.01	0.21

*i abundance is expressed as:

$$\log \epsilon(\text{Li})_{\text{LTE}} = \log[N(\text{Li})/N(\text{H})]_{\text{LTE}} + 12$$

[†]The total error was calculated using the following formula:

$$\Delta_{\text{TOTAL}} = \sqrt{\Delta_{\sigma}^2 + \Delta_{T_{\text{eff}}}^2 + \Delta_{\log g}^2 + \Delta_{\text{veiling}}^2}$$

Note. — The errors from the dispersion of the best fits to different features, Δ_{σ} , are estimated using the following formula: $\Delta_{\sigma} = \sigma/\sqrt{N}$ where σ is the standard deviation of the measurements. Total errors also take into account the uncertainties associated with the stellar parameters and the veiling.

Table 3. Element abundances ratios in the secondary star in A0620–00 and in the comparison sample

Element	$[E/Fe]_{\text{A0620-00}}$	$\Delta_{[E/Fe], \text{A0620-00}}^*$	$[E/Fe]_{\text{stars}}$	σ_{stars}	$\Delta_{\sigma, \text{stars}}$
Al	0.26	0.17	0.04	0.04	0.006
Ca	-0.04	0.13	-0.06	0.05	0.007
Ti	0.23	0.21	-0.02	0.07	0.009
Ni	0.13	0.15	-0.03	0.05	0.006

*Errors in the element abundance ratios ($[E/Fe]$) in the secondary star in A0620-00.

Note. — $[E/Fe]_{\text{stars}}$ indicate the average values calculated for stars with iron content in the range -0.06 to 0.34 corresponding to 1σ in the $[Fe/H]$ abundance of the secondary star in A0620-00. Ca, Ti and Ni for the comparison sample have been taken from 57 stars in Bodaghee et al. (2003) while Al from 36 stars in Feltzing & Gustafsson (1998). The uncertainty in the average value of element abundance ratios in the comparison sample is obtained as $\Delta_{\sigma, \text{stars}} = \sigma_{\text{stars}}/\sqrt{N}$ where σ_{stars} is the standard deviation of the measurements and N, the number of stars.

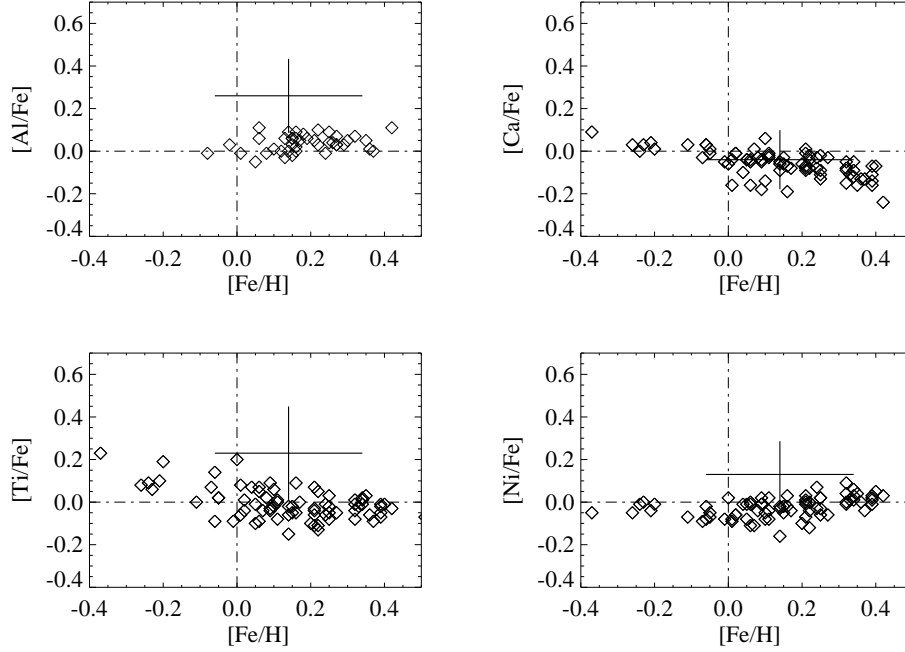


Fig. 8.— Abundances of the secondary star in A0620–00 (wide crosses) in comparison with the abundances in G and K metal-rich dwarf stars. Trends of Ca, Ni, and Ti were taken from Bodaghee et al. (2003) while Al from Feltzing & Gustafsson (1998). The size of the cross indicates the error. The dashed-dotted lines indicate solar abundance values.

and references therein):

$$M_{\text{He}} = 0.073 M_1^{1.42}$$

and

$$\log R_{\text{He}} = -1.13 + 2.26 \log M_{\text{He}} - 0.78 (\log M_{\text{He}})^2.$$

In that case, the helium core would have $M_{\text{He}} \sim 14 M_{\odot}$ and a $R_{\text{He}} \sim 2.7 R_{\odot}$, and we assume that the mass and radius of the secondary star are not significantly affected by the spiral-in. However, Hjellming & Taam (1991) have found in common envelope phase in cataclysmic variable systems that a $1.25 M_{\odot}$ secondary star could accrete $\lesssim 0.1 M_{\odot}$ from the red giant hydrogen-rich envelope (with C more depleted than N enriched, Marks & Sarna 1998). Here, we will consider that the atmosphere of the secondary star is only polluted by the ejecta in the supernova explosion of the helium core. In this case, what kind of anomalies can we expect to find at the surface of the secondary?

An important quantity in this discussion is the mass of the compact object. Gelino et al. (2001) have recently reported an estimated mass of $11 \pm 1.9 M_{\odot}$ for the compact object

in A0620–00; hence the final remnant mass in supernova model should be roughly $10 M_\odot$. The mass cuts in supernovae or even the more energetic hypernovae give rise to compact objects whose masses are not high enough to explain the high mass black hole in A0620–00 (Nakamura et al., 2001; Woosley & Weaver 1995). Therefore, the final mass of the compact object had to be generated either from a prompt and direct collapse (collapsar Type I) or, in a mild explosion with fall-back (collapsar Type II, MacFadyen et al., 2001). In the latter case, up to $\sim 5 M_\odot$ may fall back onto the collapsed remnant, turning it into a black hole. This makes it quite difficult that a significant mass fraction of iron could have escaped from the collapsing matter in the supernova event because iron is formed in the inner layers of the star. Israelian et al. (1999) found in Nova Scorpii 94 that while α -elements were enhanced Fe was not, in spite of the lower mass of the compact object ($5.4 \pm 0.3 M_\odot$, Beer & Podsiadlowski 2002) as compared with that in A0620–00. Thus, the supernova may not eject any iron, and it therefore seems quite plausible that the slightly higher than solar Fe abundance of the secondary star in A0620–00 reflects its primordial value. However, mixing of ejected material may be induced by Rayleigh–Taylor instabilities (Kifonidis et al., 2000); hence heavy elements such as ^{56}Ni may be conveyed to the outer layers in the explosion.

On the other hand, the orbital separation between the compact object and the secondary has been estimated to be $a_c = 4.47 \pm 0.27 R_\odot$ (Gelino et al., 2001). We can relate the post-supernova orbital parameters with the pre-SN parameters assuming an initially circular orbit and instantaneous spherically symmetric ejection (that is, in a time interval shorter than the orbital period). These relations are given by van den Heuvel & Habets (1984): $a_0 = a_c \mu_f$ where a_0 and a_c are the orbital separation just before the supernova and after tidal circularization of the post-SN eccentric orbit, respectively, and $\mu_f = (M_{\text{BH}} + M_2)/(M_{\text{He}} + M_2)$ where M_{BH} is the compact remnant mass. Adopting the already mentioned values ($M_{\text{BH}} \sim 10 M_\odot$, $M_{\text{He}} \sim 14 M_\odot$ and $M_2 \sim 1 M_\odot$), we find $a_0 \sim 3.3 R_\odot$. This distance is important since we assume that the secondary star was outside the He core ($R_{\text{He}} \sim 2.7 R_\odot$) of the primary before the SN explosion. Therefore, we can estimate the amount of the ejected material in a spherical explosion that could be captured by the companion as though coming from a central point. The explosion of a star as massive as the primary would have taken place only $\sim 5 \times 10^6$ yr after the formation of the system (Brunish & Truran 1982). At that time, the radius of a $1 M_\odot$ secondary star would be $\sim 1.3 R_\odot$ (D’Antona & Mazzitelli 1994). If we consider a spherically symmetric supernova explosion, taking into account the fraction of solid the angle subtended by the companion and assuming a capture efficiency, f_{capture} , of 1 (i.e., all the matter ejected within that solid angle is captured), the amount of mass deposited on the secondary would have been

$$m_{\text{add}} = \Delta M (\pi R_2^2 / 4\pi a_0^2) f_{\text{capture}} \sim 0.15 M_\odot,$$

where $\Delta M = M_{\text{He}} - M_{\text{BH}} \sim 4 M_\odot$ is the total ejected mass. This amount of ejected mass

is sufficient to explain the radial velocity of the system which is a lower limit to its *runaway* velocity (Nelemans et al., 1999).

In Tables 4 and 5 we present the expected abundances in the atmosphere of the secondary star after contamination from the progenitor of the compact object according to the above mentioned assumptions. In Table 4 we have considered two plausible masses ($1 M_{\odot}$ and $0.8 M_{\odot}$) for the secondary star at the time of the explosion of the primary and a capture efficiency factor of 1, which means that all the matter ejected within the solid angle subtended by the companion is captured. In Table 5 we have fixed the secondary mass at $0.8 M_{\odot}$ and we have considered two other efficiency factors of 0.5 and 0.1, which means that 50 and 10 per cent of the ejected mass within that solid angle is captured. We have used a $40 M_{\odot}$ spherically symmetric core-collapse explosion model ($M_{\text{He}} \sim 14 M_{\odot}$) for two different explosion energies from Umeda & Nomoto (2002 and 2003, private communication). That energy is deposited instantaneously in the central region of the progenitor core to generate a strong shock wave. The subsequent propagation of the shock wave is followed through a hydrodynamic code (Umeda & Nomoto, 2002, and references therein). In our simple model, we have assumed different mass cuts, fall-back masses and a mixing factor² that take into account the amount of fall-back matter mixed with the ejecta. We have adopted a mixing factor of 1 (i.e., all the fall-back material is well mixed with the ejecta). The amount of fall-back, M_{fallback} , is the difference between the final remnant mass, M_{BH} , and the initial remnant mass, M_{cut} . In models with $M_{\text{cut}} \leq 10 M_{\odot}$, the final remnant mass is equal to $10 M_{\odot}$ and hence the total ejected mass is $4 M_{\odot}$. Nevertheless, models with $M_{\text{cut}} > 10 M_{\odot}$ assume $M_{\text{BH}} = M_{\text{cut}}$ and do not include either fall-back or mixing. In such models, the total ejected mass, ΔM , is the difference between the final remnant mass and the helium core mass.

At the time of the explosion, the secondary was close enough to the He core ($a_0 \sim 3.3 R_{\odot}$) for the amount of matter that could have been accreted from the H-He enriched envelope after explosion to be negligible, so we do not expect a significant change in the He/H ratio in the secondary atmosphere. The hydrogen mass in the He core was $\sim 10^{-16} M_{\odot}$; therefore, we can estimate the number density of an element E in the secondary atmosphere as:

$$\left[\frac{N(\text{E})}{N(\text{H})} \right]_{\star, f} = \left[\frac{N(\text{E})_{\star} + N(\text{E})_{\text{add}}}{N(\text{H})_{\star}} \right] = \left[\frac{X(\text{E})_{\star}}{X(\text{H})_{\star}} 10^{[\text{E}/\text{H}]_{\dagger, i}} + \frac{X(\text{E})_{\text{add}}}{X(\text{H})_{\star}} \frac{m_{\text{add}}}{m_{\text{conv}}} \right] \frac{m_{\text{H}}}{m_{\text{E}}},$$

²Other detailed explosion models have been considered in the analysis of over-abundances of the secondary star in Nova Sco 94 by Podsiadlowski *et al.* (2002).

Table 4. Expected element abundances of the secondary star in A0620–00

Element	[E/H] [‡]		[E/H] [*]															
$\varepsilon(10^{51}\text{erg})$			1								30							
$M_{\text{cut}}(M_{\odot})$			1.96	5	7	10	11	12	12.5	12.9	2.03	5	7	10	11	12	12.5	12.9
M_2			1 M_{\odot}															
Al	0.40	0.21	1.50	1.52	1.50	1.40	1.12	0.68	0.37	0.22	1.36	1.47	1.51	1.40	1.12	0.70	0.38	0.22
Ca	0.10	0.09	0.88	0.12	0.12	0.13	0.12	0.11	0.11	0.10	1.26	0.14	0.12	0.12	0.11	0.10	0.10	0.10
Ti	0.37	0.13	0.82	0.31	0.31	0.29	0.23	0.18	0.16	0.15	1.47	0.31	0.31	0.30	0.23	0.18	0.16	0.15
Fe	0.14	0.14	0.94	0.17	0.17	0.17	0.17	0.16	0.16	0.15	1.26	0.16	0.16	0.17	0.16	0.15	0.15	0.15
Ni	0.27	0.12	1.12	0.49	0.48	0.44	0.33	0.23	0.18	0.15	1.47	0.54	0.52	0.52	0.41	0.31	0.27	0.23
O	1.16	1.18	1.17	1.11	0.90	0.61	0.39	0.15	1.12	1.20	1.17	1.11	0.89	0.61	0.39	0.15
Mg	1.20	1.18	1.16	1.07	0.83	0.50	0.30	0.15	1.13	1.24	1.21	1.10	0.87	0.57	0.39	0.25
Si	1.05	0.41	0.40	0.36	0.27	0.19	0.16	0.15	1.35	1.04	0.54	0.37	0.27	0.19	0.17	0.15
S	0.93	0.19	0.19	0.19	0.18	0.16	0.16	0.15	1.32	0.91	0.22	0.19	0.17	0.16	0.15	0.15
C	0.82	0.87	0.86	0.84	0.68	0.50	0.37	0.16	0.69	0.78	0.85	0.84	0.68	0.50	0.37	0.17
M_2			0.8 M_{\odot}															
Al	0.40	0.21	1.43	1.45	1.43	1.33	1.05	0.63	0.35	0.22	1.29	1.40	1.43	1.33	1.06	0.65	0.36	0.22
Ca	0.10	0.09	0.82	0.12	0.12	0.12	0.11	0.11	0.10	0.10	1.19	0.13	0.11	0.12	0.11	0.10	0.10	0.10
Ti	0.37	0.13	0.76	0.29	0.29	0.27	0.22	0.17	0.16	0.14	1.40	0.29	0.29	0.27	0.22	0.17	0.16	0.15
Fe	0.14	0.14	0.88	0.16	0.16	0.17	0.16	0.16	0.15	0.15	1.19	0.16	0.16	0.16	0.15	0.15	0.15	0.15
Ni	0.27	0.12	1.05	0.45	0.44	0.41	0.30	0.21	0.17	0.14	1.40	0.50	0.48	0.48	0.38	0.29	0.25	0.22
O	1.10	1.11	1.10	1.05	0.83	0.56	0.36	0.14	1.05	1.14	1.10	1.04	0.83	0.56	0.36	0.14
Mg	1.13	1.11	1.09	1.01	0.77	0.46	0.28	0.15	1.06	1.17	1.14	1.04	0.81	0.53	0.36	0.24
Si	0.98	0.38	0.37	0.34	0.25	0.18	0.16	0.15	1.28	0.97	0.50	0.34	0.26	0.19	0.16	0.15
S	0.87	0.18	0.18	0.19	0.17	0.16	0.15	0.15	1.25	0.85	0.21	0.18	0.17	0.16	0.15	0.15
C	0.76	0.81	0.80	0.79	0.62	0.46	0.34	0.16	0.64	0.72	0.79	0.78	0.62	0.46	0.34	0.16

*Secondary star abundances relative to solar.

‡This column shows observed abundances of the secondary star in A0620–00.

†This column shows the average abundances in stars of the comparison sample (see also Table 3).

Note. — Expected abundances in the secondary atmosphere contaminated with nucleosynthetic products of a 40 M_{\odot} spherically symmetric core-collapse explosion model ($M_{\text{He}} \sim 14 M_{\odot}$) for two different explosion energies. M_{cut} is the mass cut assumed for each model. In every model, the final remnant mass, M_{BH} , is fixed at 10 M_{\odot} , except those models with $M_{\text{cut}} = 11, 12, 12.5$, and 12.9 M_{\odot} . Mixing factors between the fall-back matter and the ejecta have been adopted equal to 1. In every model, the amount of fall-back, M_{fallback} , is the difference between M_{BH} and M_{cut} . The capture efficiency, f_{capture} , is fixed at 1. Elements which have not been analyzed (i.e. O, Mg, S, Si and C) have been scaled up with $[\text{Fe}/\text{H}]_{\dagger,i} = 0.14$.

Table 5. Expected element abundances of the secondary star in A0620–00

Element	[E/H] [‡]	[E/H] [‡]	[E/H] [*]															
$\varepsilon(10^{51}\text{erg})$	1												30					
$M_{\text{cut}}(M_{\odot})$	1.96	5	7	10	11	12	12.5	12.9	2.03	5	7	10	11	12	12.5	12.9		
f_{capture}	0.5																	
Al	0.40	0.21	1.15	1.18	1.15	1.06	0.81	0.47	0.28	0.21	1.02	1.13	1.16	1.06	0.81	0.48	0.29	0.22
Ca	0.10	0.09	0.59	0.10	0.10	0.11	0.10	0.10	0.10	0.10	0.92	0.11	0.10	0.10	0.10	0.10	0.09	0.09
Ti	0.37	0.13	0.55	0.22	0.22	0.21	0.18	0.15	0.14	0.14	1.12	0.22	0.22	0.21	0.18	0.15	0.14	0.14
Fe	0.14	0.14	0.65	0.15	0.15	0.15	0.15	0.15	0.15	0.15	0.92	0.15	0.15	0.15	0.15	0.14	0.14	0.14
Ni	0.27	0.12	0.80	0.32	0.31	0.29	0.23	0.17	0.15	0.14	1.12	0.35	0.34	0.34	0.27	0.22	0.19	0.18
O	0.84	0.86	0.84	0.80	0.61	0.40	0.26	0.14	0.80	0.88	0.84	0.79	0.61	0.40	0.26	0.14
Mg	0.87	0.86	0.84	0.76	0.56	0.33	0.21	0.15	0.81	0.90	0.88	0.79	0.59	0.38	0.26	0.19
Si	0.74	0.28	0.27	0.25	0.20	0.16	0.15	0.15	1.00	0.73	0.36	0.25	0.20	0.16	0.15	0.15
S	0.64	0.16	0.16	0.16	0.16	0.15	0.15	0.15	0.98	0.63	0.18	0.16	0.15	0.15	0.15	0.14
C	0.55	0.59	0.59	0.57	0.45	0.33	0.25	0.15	0.46	0.52	0.58	0.57	0.45	0.33	0.25	0.15
f_{capture}	0.1																	
Al	0.40	0.21	0.62	0.63	0.62	0.55	0.41	0.28	0.22	0.21	0.53	0.60	0.62	0.56	0.41	0.28	0.23	0.21
Ca	0.10	0.09	0.25	0.09	0.09	0.09	0.09	0.09	0.09	0.09	0.42	0.09	0.09	0.09	0.09	0.09	0.09	0.09
Ti	0.37	0.13	0.25	0.15	0.15	0.15	0.14	0.14	0.13	0.13	0.57	0.15	0.15	0.15	0.14	0.14	0.13	0.13
Fe	0.14	0.14	0.30	0.14	0.14	0.14	0.14	0.14	0.14	0.14	0.44	0.14	0.14	0.14	0.14	0.14	0.14	0.14
Ni	0.27	0.12	0.37	0.18	0.17	0.17	0.15	0.14	0.14	0.13	0.57	0.19	0.18	0.18	0.16	0.15	0.15	0.14
O	0.40	0.40	0.40	0.37	0.28	0.21	0.17	0.14	0.38	0.42	0.40	0.37	0.28	0.21	0.17	0.14
Mg	0.41	0.41	0.39	0.35	0.26	0.18	0.16	0.14	0.38	0.43	0.42	0.37	0.28	0.20	0.17	0.15
Si	0.34	0.17	0.17	0.16	0.15	0.14	0.14	0.14	0.50	0.34	0.19	0.16	0.15	0.14	0.14	0.14
S	0.30	0.14	0.14	0.14	0.14	0.14	0.14	0.14	0.48	0.29	0.15	0.14	0.14	0.14	0.14	0.14
C	0.26	0.28	0.27	0.27	0.22	0.18	0.16	0.14	0.22	0.25	0.27	0.27	0.22	0.18	0.17	0.14

*Secondary star abundances relative to solar.

[‡]This column shows observed abundances of the secondary star in A0620–00.

[†]This column shows the average abundances in stars of the comparison sample (see also Table 3).

Note. — The same as in Table 4 but the secondary mass is fixed at $0.8 M_{\odot}$. However, the capture efficiency, f_{capture} , is lower than 1. Its values are 0.5 which means that only half of the matter ejected within the solid angle subtended by the companion is captured whereas 0.1 means that only 10 per cent is captured.

where $N(\text{E})_\star$ and $N(\text{H})_\star$ are the number density of elements E and H in the convective zone of the star, $N(\text{E})_{\text{add}}$ the number density of E in the captured matter, m_{add} , by the companion, $X(\text{E})_\star$ and $X(\text{H})_\star$ the mass fractions of E and H in the convective zone, $X(\text{E})_{\text{add}}$ is the mass fraction of E in the captured matter, m_{conv} is the mass of the convective zone, and m_{H} and m_{E} the atomic masses of H and E, respectively. The mass of the convective zone was fixed at $m_{\text{conv}} = 0.652$ and $0.667 M_\odot$ from the evolutionary tracks for a 1 and $0.8 M_\odot$ secondary stars, respectively, with an age of $\sim 5 \times 10^6$ yr (D’Antona & Mazzitelli 1994).

The original element mass fractions in the secondary star were assumed to be solar from Anders & Grevesse (1989) and we have also considered an explosion model from a solar metallicity progenitor. However, in order to take into account that the initial iron content of the star was probably higher than solar ($[\text{Fe}/\text{H}]_{\dagger,i} = 0.14$) we scaled up the expected abundances with $[\text{E}/\text{H}]_{\dagger,i}$ which is the average element abundance in the comparison sample using data shown in Fig. 8 (see Table 3). Expected abundances shown in Table 4 and 5 were calculated using the following formula:

$$[\text{E}/\text{H}]_{\star,f} = \log \left[\frac{N(\text{E})}{N(\text{H})} \right]_{\star,f} - \log \left[\frac{N(\text{E})}{N(\text{H})} \right]_\odot$$

It is clearly seen that only models with mass cuts as high as $11 M_\odot$ can fit the abundances of the secondary star within the error bars. In models with lower mass cuts, the amount of Al in the ejecta is too high in comparison with the other heavy elements analyzed. Even under strong assumptions such as large amounts of fall-back matter, M_{fallback} , and/or mixing efficiency fixed at 1, it is not possible to get good fits to the observed abundance values for mass cuts below $11\text{--}12 M_\odot$ depending on the capture efficiency assumed. This is independent of the explosion energy, ε , since this parameter has little influence on the Al yield at any mass cut. It does not depend on the mass of the secondary. In summary, the moderate over-abundances of Ti, Ni, and especially Al could be explained if there were an explosion event of a star of initial mass $\sim 40 M_\odot$ with a helium core of $\sim 14 M_\odot$ that led to the formation of a black hole with a mass of approximately $11\text{--}12.5 M_\odot$. As in the case of Nova Sco 94 (Israelian et al., 1999), we find signatures in the secondary of A0620–00 that suggest the formation of the black hole as a consequence of an explosive event.

However, as we have already mentioned in §1, many uncertainties still remain in supernova explosion models and in the evolution of LMXBs. For instance, a capture efficiency as high as 1 may not be adequate since simulations of type Ia SNe suggest that the supernova blast wave may induce mass-loss in the secondary instead of matter accretion (Marietta et al., 2000). On the other hand, the assumption of spherical symmetry is not generally expected for hypernova or collapsar models, in particular those associated with gamma-ray

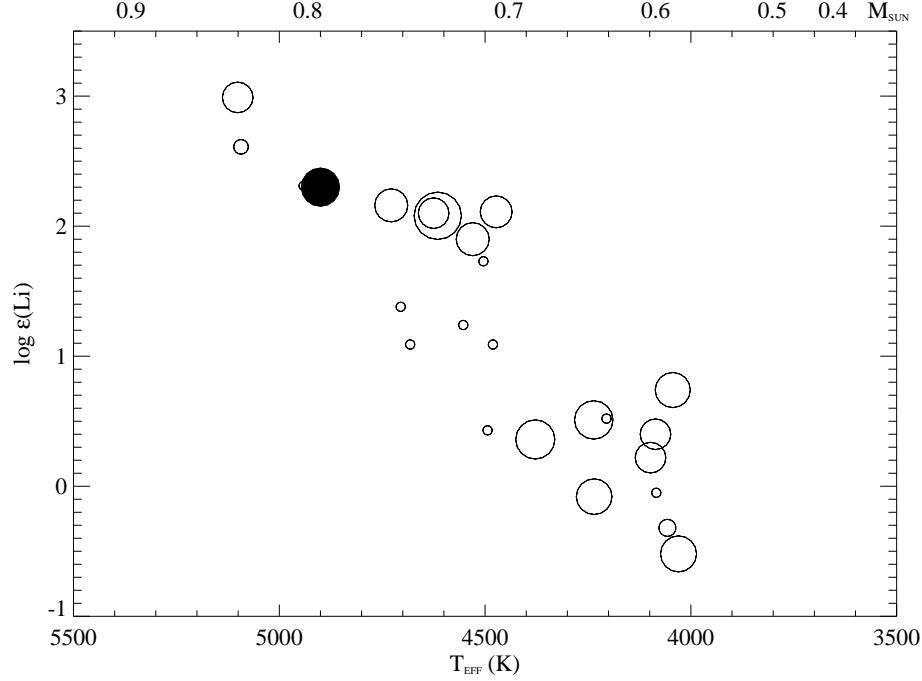


Fig. 9.— Li abundance of the secondary star in A0620–00 (filled circle) in comparison with the abundances of different rotating Pleiades dwarf stars versus effective temperature from García López et al. (1994). The sizes of the circles are related to $v \sin i$. Stellar masses have been assigned following the evolutionary tracks of D’Antona & Mazzitelli (1994) for 10^8 yr.

burst (MacFadyen & Woosley, 1999). Maeda et al. (2002) have studied nucleosynthesis in aspherical explosions and found that the chemical composition of the ejecta is strongly dependent on direction. In particular, Fe is mainly ejected in the polar direction, whereas O and other alpha-elements (e.g. Si, S, Mg) are preferentially ejected near the equatorial plane. Therefore, it would be interesting to analyze other elements such as O, Mg, and C, which are enhanced in many of the model computations in Table 4 and 5, even at high mass cuts. We note that Orosz et al. (2001) have also found overabundances (by a factor 2–10 with respect to solar) of some of these elements in the secondary star of the LMXB system J1819.3–2525 (V4641 Sgr).

4.2. Li abundance

The abundance of lithium in the secondary star in A0620–00 is substantially higher than in field main sequence stars of the same mass ($\sim 0.7 M_{\odot}$) but similar to that of Pleiades stars

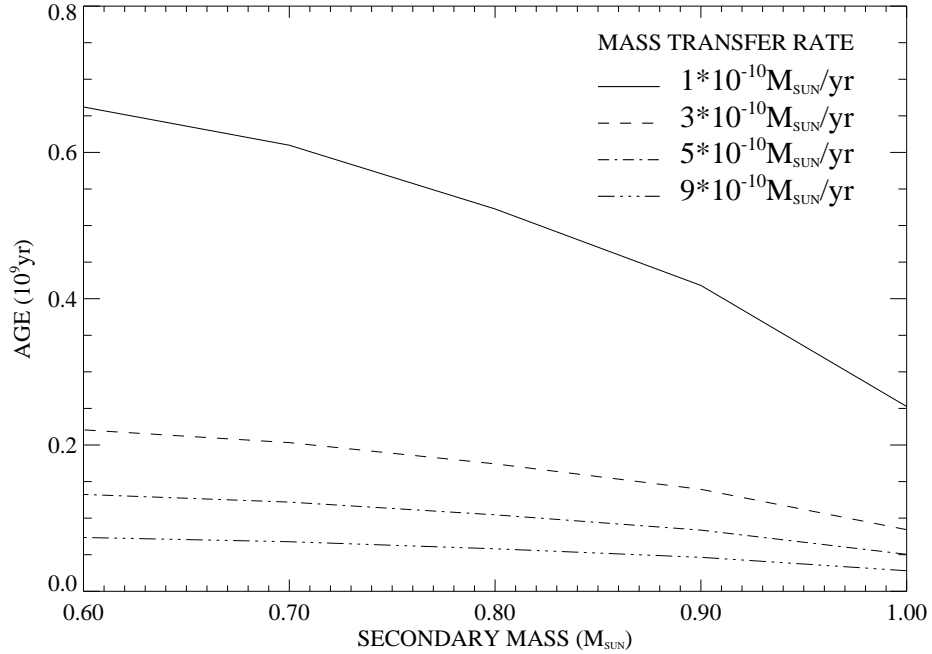


Fig. 10.— Upper limit to the age of the A0620–00 system according to the Li abundance of the secondary star versus stellar masses of the secondary star, assuming different mass transfer rates. Stellar masses have been assigned according to the evolutionary tracks of D’Antona & Mazzitelli (1994) for 10^8 yr.

of comparable mass and rotational velocity (see Fig. 9). Convective mixing during pre-main sequence and main sequence evolution is expected to produce significant lithium depletion in the atmospheres of such stars, thus a possible explanation for the Li over-abundance in the secondary is that the A0620–00 system is as young as the Pleiades cluster (i.e., $\sim 7\text{--}15 \times 10^7$ yr). This appears to be in conflict with the evolutionary scenario proposed by de Kool et al. (1987), where an age of a few times 10^9 yr is assumed. However, Naylor & Podsiadlowski (1993) have argued, based on the galactic distribution of LMXBs, that these systems are associated with the Galactic disk, and probably have an age of only 10^7 to 10^8 yr. If the lifetime were this short, the mass loss from the companion would not have been relevant since the present mass transfer rate is $\dot{M}_2 \sim 10^{-10} M_{\odot} \text{ yr}^{-1}$ (McClintock et al., 1995) although it may not necessarily be stable in the course of the whole binary lifetime ($\dot{M}_2 \sim 10^{-9}\text{--}10^{-10} M_{\odot} \text{ yr}^{-1}$, Ergma & Fedorova 1998).

It is possible to constrain the age of the system using the current Li abundance and plausible mass transfer rates. Let us assume in what follows that there is no mechanism able to enrich the atmosphere of the secondary star with freshly synthesized Li nuclei. If

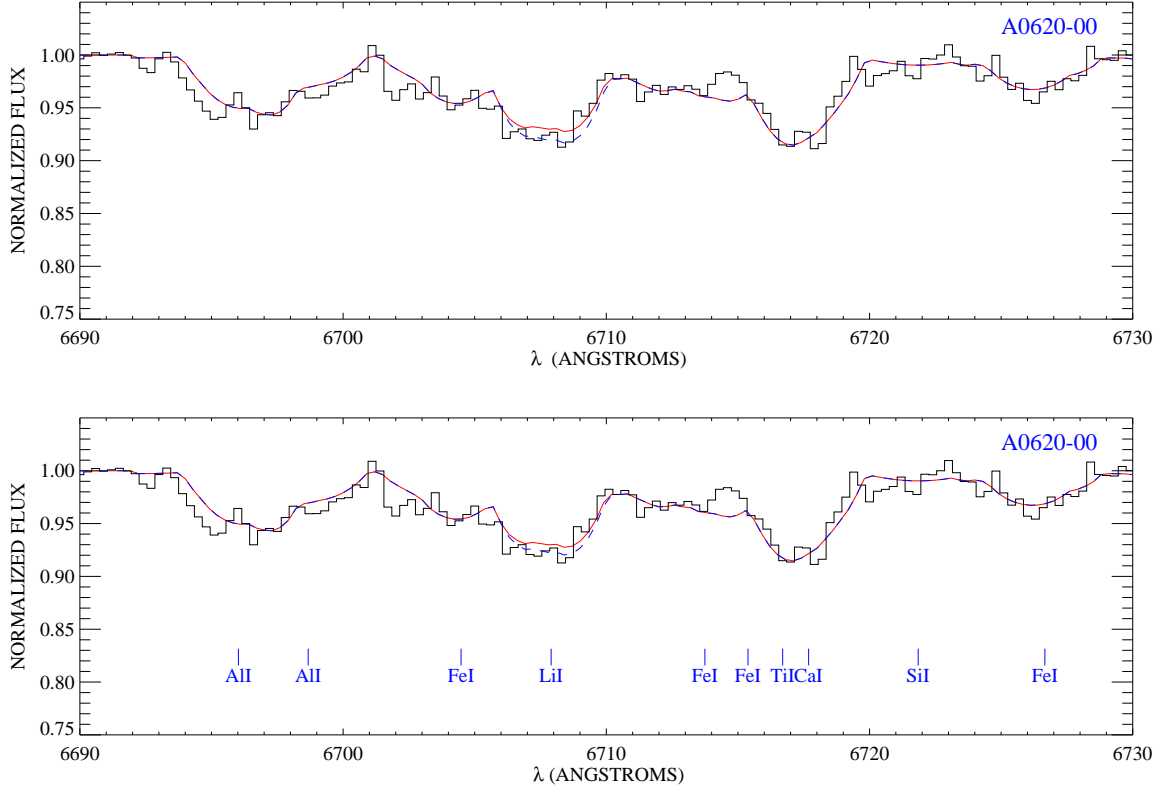


Fig. 11.— Best synthetic spectral fits to the UVES spectrum of the secondary star in the A0620-00 system considering only ${}^7\text{Li}$ in the spectral line Li I 6708. Superimposed to them were displayed different spectral synthesis, fixed Li abundance, for ${}^7\text{Li}/{}^6\text{Li} = 2$ (dashed line in top panel) and for ${}^7\text{Li}/{}^6\text{Li} = 5$ (dashed line in bottom panel).

the initial mass of the secondary star were smaller than $1 M_{\odot}$ Li could survive only in the outer layers, i.e., above the bottom of the convective zone. In a solar type star, the mass of the convective zone is $0.03 M_{\odot}$, and, given the range of plausible mass transfer rates for the secondary, such a mass would be transferred to the compact object in less than 0.3 Gyr, leaving the atmosphere of the secondary completely free of Li nuclei, which we see cannot be the case. In Fig. 10 we show how this simple argument constrains the age of the system for different mass transfer rates and initial secondary masses. In summary, the more massive the secondary star and the higher the mass transfer rate are, the stringent the upper limit to the age of the system that can be imposed. The curves in Fig. 10, in fact, give conservative upper limits to the age, in particular for the lower mass range, since we have not taken into account that some Li depletion caused by convective mixing may also have occurred. We note that we have not considered values for the initial mass of the secondary above $1 M_{\odot}$.

because under the mass transfer rates considered such stars cannot lead to an object of the present mass and preserve the required amount of Li.

High Li abundances have been noticed by Martín et al. (1994) in other LMXBs such as Cen X-4 and V404 Cyg. These authors suggested as an alternative explanation of youth the existence of a production mechanism of lithium. Either early in the evolution of the system during the supernova explosion of the primary progenitor; or a continuing process such as α – α reactions during the repeated strong outbursts that characterize transient X-ray binaries. If, indeed, fresh Li is synthesized and trapped in the atmosphere, the above arguments to constrain the age cannot hold. It is thus, very important to find a way of disentangling the origin of the high Li abundances observed. The spallation mechanism would produce considerable amounts of the ^6Li isotope with isotopic ratios as low as $^7\text{Li}/^6\text{Li} = 5$. However, trials using a $^7\text{Li}/^6\text{Li}$ isotopic ratio of 5 and 2 were performed (see Fig. 11), but they gave a slightly worse numerical fit to the observed spectrum than the case of pure ^7Li . Higher S/N spectroscopic observations will be needed to test the spallation scenario. Recently, Li has been detected in the companion of the millisecond pulsar J1740–5340 in the globular cluster NGC 6397 (Sabbi et al. 2003). The secondary is a turn-off star which has lost most of its mass and thus most of its initial lithium content. The high Li abundance measured in this star suggests that actually some Li production may take place in these systems.

5. Conclusions

We have obtained a high quality spectrum of the secondary star in A0620–00 and derived atmospheric chemical abundances. We have set up a technique that provides a determination of the stellar parameters taking into account any possible veiling from the accretion disk. We find $T_{\text{eff}} = 4900 \pm 150$ K, $\log g = 4.2 \pm 0.3$, and a veiling (defined as $F_{\text{disk}}/F_{\text{cont,star}}$) of less than 15 per cent at 5000 Å and decreasing towards longer wavelengths. Assuming a mass for the secondary of $M_2 = 0.68 \pm 0.18 M_{\odot}$, the estimated surface gravity leads to a stellar radius of $R_2 = 1.1 \pm 0.4 R_{\odot}$, consistent with the size of the Roche lobe for the secondary given by Gelino et al. (2001).

The abundances of Fe, Ca, Ti, Al, and Ni are slightly higher than solar. The abundance ratios of each element with respect to Fe were compared with these ratios in late-type main sequence metal-rich stars. Moderate anomalies for Ti, Ni, and especially Al have been found. A comparison with element yields from spherically symmetric supernova explosion models suggests that the secondary star captured part of the ejecta from a supernova that also originated the compact object in A0620–00. The abundances can be explained if a progenitor with a $\sim 14 M_{\odot}$ helium core exploded with a mass cut in the range 11–12.5 M_{\odot} ,

such that no significant amount of iron could escape from the collapse of the inner layers. Elements such as O, Mg, Si, S, and C, with unavailable transitions in our spectrum, will be studied to confirm this scenario.

The Li abundance in the secondary star in A0620–00 is dramatically enhanced in comparison with field late-type main sequence stars, possibly indicating either that this is a young system ($\sim 0.5\text{--}2 \times 10^8$ yr), or the existence of a Li production-preservation mechanism, such as the α – α reactions, which have to be tested analyzing the $^7\text{Li}/^6\text{Li}$ isotopic ratio using future higher S/N optical spectroscopic observations.

6. Acknowledgements

We are grateful to Hideyuki Umeda and Ken’ichi Nomoto for sending us their explosion models and several programs for our model computations, and for helpful discussions. We would also like to thank José Acosta Pulido for his help in the stellar and accretion disk parameter program for searching the best stellar atmospheric model. We also thank the referee for useful comments. This work has made use of the VALD database and IRAF facilities and have been partially financed by the Spanish Ministry project AYA2001-1657.

REFERENCES

- Anders, E., & Grevesse, N. 1989, *Geochim. Cosmochim. Acta*, 53, 197
- Beer, M., & Podsiadlowski, Ph. 2002, *MNRAS*, 331, 351
- Bodaghee, A., Santos, N. C., Israelian, G., & Mayor, M. 2003, *A&A*, 404, 715
- Brown, G. E., Lee, C.-H., & Bethe, H. A. 1999, *NewA*, 4, 313
- Brown, G. E., Lee, C.-H., Wijers, R. A. M. J., Lee, H. K., Israelian, G., & Bethe, H. A. 2000, *NewA*, 5, 191
- Brunish, W. M., & Truran, J. W. 1982, *ApJS*, 49, 447
- Chiosi C., & Maeder A. 1986, *ARA&A*, 24, 329
- Casares et al. 2004, in preparation
- D’Antona, F., & Mazzitelli, I. 1994, *ApJS*, 90, 467

- Elvis, M., Page, C. G., Pounds, K. A., Ricketts, M. J., & Turner, M. J. L. 1975, *Nature*, 257, 656
- Ergma, E., & Fedorova, A. 1998, *A&A*, 338, 69
- Feltzing, S., & Gustafsson, B. 1998, *A&AS*, 129, 237
- Fryer, C. L., & Warren, M. S. 2002, *ApJ*, 574, L65
- García López, A., Rebolo, R., & Martín, E. L. 1994, *A&A*, 282, 518
- Gelino, D. M., Harrison, T. E., & Orosz, J. A. 2001, *ApJ*, 122, 2668
- Hachisu, I., Matsuda, T., Nomoto, K., & Shigeyama, T. 1991, *ApJ*, 368, L27
- Heger, A., Langer, N., & Woosley, S. E. 2000, *ApJ*, 528, 368
- Herant, M., & Woosley, S. E., *ApJ*, 425, 814 (1994)
- Herant, M., Benz, W., Hix, W. R., Fryer, C. L., & Colgate, S. A. 1994, *ApJ*, 435, 339
- Herbig, G. H. 1995, *ARA&A*, 33, 19
- van den Heuvel, & E. P. J., Habets, G. M. H. J. 1984, *Nature*, 309, 598
- Hjellming, M. S., & Taam, R. E. 1991, *ApJ*, 370, 709
- Israelian, G., Rebolo, R., Basri, G., Casares, J., & Martín, E. L. 1999, *Nature*, 401, 142
- Kalogera, V., & Webbink, R. F. 1998, *ApJ*, 493, 351
- Kifonidis, K., Plewa, T., Janka, H.-Th., & Mller, E. 2000, *A&A*, 531, 123
- de Kool, M., van den Heuvel, E. P. J., & Pylyser, E. 1987, *A&A*, 183, 47
- Kurucz, R. L., Furenlid, I., Brault, J., & Testerman, L. 1984, *Solar Flux Atlas from 296 to 1300 nm*, NOAO Atlas 1 (Cambridge: Harvard Univ. Press)
- Langer, N. 1991, *A&A*, 248, 531
- MacFadyen, A. I., & Woosley, S. E. 1999, *ApJ*, 524, 262
- MacFadyen, A. I., Woosley, S. E., & Heger, A. 2001, *ApJ*, 550, 410
- Maeda, K., Nakamura, T., Nomoto, K., Mazzali, P. A., Patat, F., & Hachisu, I. 2002, *ApJ*, 565, 405

- Maeder A., & Meynet, G. 2000, ARA&A, 38, 143
- Marietta, E., Burrows, A., & Fryxell, B. 2000, ApJS, 128, 615
- Marks, P. B., & Sarna, M. J. 1998, MNRAS, 301, 699
- Marsh, T. R., Robinson, E. L., & Wood, J. H. 1994, MNRAS, 266, 137
- Martín, E. L., Rebolo, R., Casares, J., & Charles, P. A. 1994, ApJ, 435, 791
- McClintock, J. E., & Remillard, R. A. 1986, ApJ, 308, 110
- McClintock, J. E., Horne, K., & Remillard, R. A. 1995, ApJ, 442, 358
- McClintock, J. E., & Remillard, R. A. 2000, ApJ, 531, 956
- Meynet, G., & Maeder, A. 2003, A&A, 404, 975
- Mirabel, I. F., Mignani, R., Rodrigues, I., Combi, J. A., Rodríguez, L. F., & Guglielmetti, F. 2002, A&A, 395, 595
- Murdin, P., Allen, D. A., Morton, D. C., Whelan, J. A. J., & Thomas, R. M. 1980, MNRAS, 192, 709
- Nakamura, T., Umeda, Hideyuki, Iwamoto, K., Nomoto, K., Hashimoto, M., Hix, W. R., & Thielemann, F. K. 2001, ApJ, 555, 880
- Naylor, T., Podsiadlowski, Ph. 1993, MNRAS, 262, 929
- Nelemans, G., Tauris, T. M., & van den Heuvel, E. P. J. 1999, A&A, 352, L87
- Nugis, T., & Lamers, H.J.G.L.M. 2000, A&A, 360, 227
- Oke, J. B. 1977, ApJ, 217, 181
- Orosz, J. A., Kuulkers, E., van der klis, M., McClintock, J. E., Garcia, M. R., Callanan, P. J., Baylin, C. D., Jain, R. K., & Remillard, R. A. 2001, ApJ, 555, 489
- Podsiadlowski, P., Nomoto, K., Maeda, K., Nakamura, T., Mazzali, P., & Schmidt, B. 2002, ApJ, 567, 491
- Portegies Zwart, S. M., Verbunt, F., & Ergma, E. 1997, A&A, 321, 207
- Sabbi, E., Gratton, R. G., Bragaglia, A., Ferraro, F. R., Possenti, A., Camilo, F., & D’Amico, N. 2003, A&A, 412, 829

- Shahbaz, T., Naylor, T., & Charles, P. A. 1994, MNRAS, 268, 756
- Shahbaz, T., Bandyopadhyay, R. M., & Charles, P. A. 1999, A&A, 346, 82
- Snedden, C. 1973, PhD Dissertation (Univ. of Texas at Austin)
- Umeda, H., & Nomoto, K. 2002, ApJ, 565, 385
- Umeda, H., & Nomoto, K. 2003, Nature, 422, 871
- Woosley, S. E., Langer, N., & Weaver, T. A. 1993, ApJ, 411, 823
- Woosley, S. E., & Weaver, T. A. 1995, ApJS, 101, 181
- Woosley, S. E., Langer, N., & Weaver, T. A. 1995, ApJ, 448, 315